

## PROGRESS IN DESIGN OF DEMO-FNS HYBRID FACILITY

Yu.S. Shpanskiy and DEMO-FNS project team  
NRC "Kurchatov Institute  
Moscow, Russian Federation  
Email: [Shpanskiy\\_YS@nrcki.ru](mailto:Shpanskiy_YS@nrcki.ru)

### *DEMO-FNS Project Team*

B.V. Kuteev<sup>1</sup>, Yu.S. Shpanskiy<sup>1</sup>, R.S. Afanassenko, S.S. Ananiev<sup>1</sup>, E.D. Dlugach<sup>1</sup>, A.Yu. Dnestrovskij<sup>1</sup>, D.P. Ivanov<sup>1</sup>, R.R. Khairutdinov<sup>1</sup>, V.I. Khripunov<sup>1</sup>, A.V. Klischenko<sup>1</sup>, A.S. Kukushkin<sup>1</sup>, V.E. Lukash<sup>1</sup>, V.V. Lukianov<sup>1</sup>, S.Yu. Medvedev<sup>1</sup>, A.A. Morozov, A.Yu. Pashkov<sup>1</sup>, V.S. Petrov<sup>1</sup>, A.B. Sivak<sup>1</sup>, M.N. Shlenskiy, A.V. Spitsyn<sup>1</sup>, A.V. Zhirkin<sup>1</sup>,  
V.A. Belyakov<sup>2</sup>, E.N. Bondarchuk<sup>2</sup>, V.V. Chernenok, A.A. Kavin<sup>2</sup>, M.V. Khohlov<sup>2</sup>, S.V. Krasnov<sup>2</sup>, A.N. Labusov<sup>2</sup>, A.B. Mineev<sup>2</sup>, V.P. Muratov<sup>2</sup>, I.Yu. Rodin<sup>2</sup>, V.A. Trofimov<sup>2</sup>, E.R. Zapretilina<sup>2</sup>, I.V. Danilov<sup>3</sup>, A.V. Lopatkin<sup>3</sup>, I.B. Lukasevitch<sup>3</sup>, V.E. Popov<sup>3</sup>, Yu.S. Strebkov<sup>3</sup>, A.G. Sysoev<sup>3</sup>, P.R. Goncharov<sup>4</sup>, V.Yu. Sergeev<sup>4</sup>

<sup>1</sup>National Research Center "Kurchatov Institute", Moscow, Russia

<sup>2</sup>Efremov Institute, Sankt-Petersburg, Russia

<sup>3</sup>NIKIET, Moscow, Russia

<sup>4</sup>Peter the Great SPbPU, St.Petersburg, Russia

### **Abstract**

Further development of a fusion-fission hybrid facility based on superconducting tokamak DEMO-FNS [1] continues in Russia for integrated commissioning of steady-state and nuclear fusion technologies at the power level up to 40 MW fusion and 400 MW fission reactions. This facility is considered as the main source of technological and nuclear scientific information in the RF National program on controlled fusion and plasma technologies that is currently being developed and submitted to the authorities for approval.

### 1. INTRODUCTION

The DEMO-FNS facility employs a conventional tokamak with superconducting electromagnetic system as an intense 14 MeV neutron source. The design of current stage is aimed at reaching steady state operation of the plant with the neutron wall loading of  $\sim 0.2$  MW/m<sup>2</sup>, the lifetime neutron fluence of  $\sim 2$  MWa/m<sup>2</sup>, with the surface area of the active cores and tritium breeding blanket  $\sim 100$  m<sup>2</sup>. These plant parameters are sufficient for material and component testing in the fusion neutron spectrum as well as for the development of hybrid energy generation, transmutation technology, production of nuclear fuels (including U-233 from Th-232) and tritium. Earlier DEMO-FNS design options were presented at the FEC-2014 and FEC-2016 conferences [1], [2]. This report summarizes the work performed in 2017-2018. The design goals were concentrated on the development of new simulation tools and plasma scenarios, improvement of characteristics of enabling systems, integrated device design implementing upgraded and new systems, such as first wall (FW), divertor, active core, tritium breeding blanket (TBB), NBI, fuelling and pumping, heat transfer, remote handling.

Although the major dimensions of the tokamak device were fixed (major radius  $R = 3.2$  m, minor radius  $a = 1.0$  m, elongation 2.7, triangularity 0.5), optimization of port configurations for additional heating and current drive was made and additional ports for remote handling of active cores were added in the design. New design of the facility with separate maintenance and remote handling of multiple active cores and tritium breeding blanket with minimal maintenance requirements was developed.

DEMO-FNS tokamak general view is shown in Fig.1. Simplification of the NBI system and its gas loop in DEMO-FNS complex is very desirable taking into account high power and gas flows circulating in it. Since the option of NBI operation with D-beams was as chosen as basic it became necessary to optimize the composition of DT core plasma. Core plasma modelling showed that the neutron yield is maximal and overcoming by a factor of 1.3 that of homogeneity fuel mixture if the tritium/deuterium density ratio is 1.5-2.3. The neutron fraction produced in beam-plasma reactions grows up with the T/D ratio from equal fractions, in the optimal mode matching that due to thermonuclear reactions.

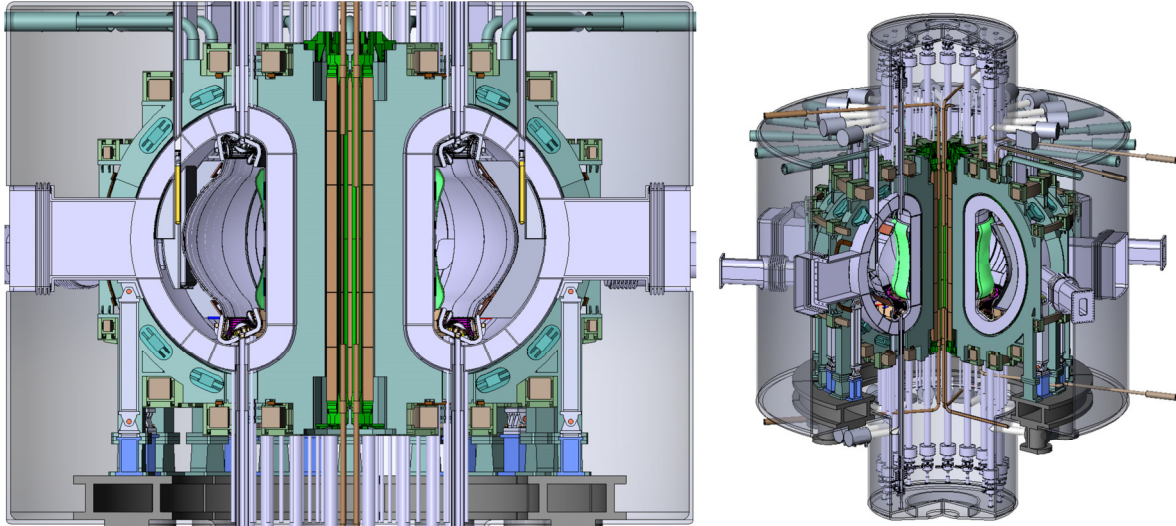


FIG. 1. DEMO-FNS tokamak general view with vertical ports for active cores.

## 2. CORE PLASMA MODELING

### 2.1. Tritium fraction influence on fusion power

The fusion power produced by both plasma-plasma and beam-plasma interactions is shown in Fig.2 for the case of pure deuterium beam in dependence of the tritium fraction in plasma. For the case of maximal total fusion power with a tritium fraction equal to 0.7 both contributions from plasma-plasma and beam-plasma interactions are obtained to be equal. The difference is clear with the case of mixed D-T beam when the maximal fusion power is reached with the tritium fraction equal to 0.5 with the plasma-plasma contribution twice as much beam-plasma contribution.

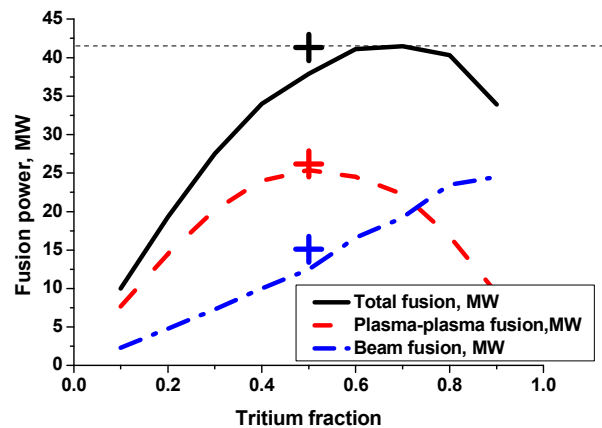


FIG. 2. Total fusion power (black solid line) and fusion power produced by plasma-plasma (dashed red line) and beam-plasma (dot-dashed blue line) interactions vs tritium fraction in the thermal component in D-beam case. Crosses show results of D-T beam case.)

### 2.2. Major disruption in FNS

In order to calculate the electromagnetic loads in the conductive filaments of the vacuum vessel (VV) and the passive structure (PSin, PSout) during major disruption, a modeling of the FNS plasma evolution during "hot" VDE, which results from a breaking of the plasma position control system, is performed using the DINA [3] code. Fig. 2a shows the evolution of the main parameters of the FNS plasma in the VDE process, during which the uncontrolled hot plasma in the divertor configuration begins to move in the vertical direction. During the motion, it sits on the limiter, after which the process of the poloidal plasma surface shrinking begins (Fig. 2), as a result of which the value of the magnetic stability margin of the plasma at its boundary  $q_{95}$  decreases. With a decrease in  $q_{95}$  to a critical value  $q^* = 2.5$ , a major disruption occurs.

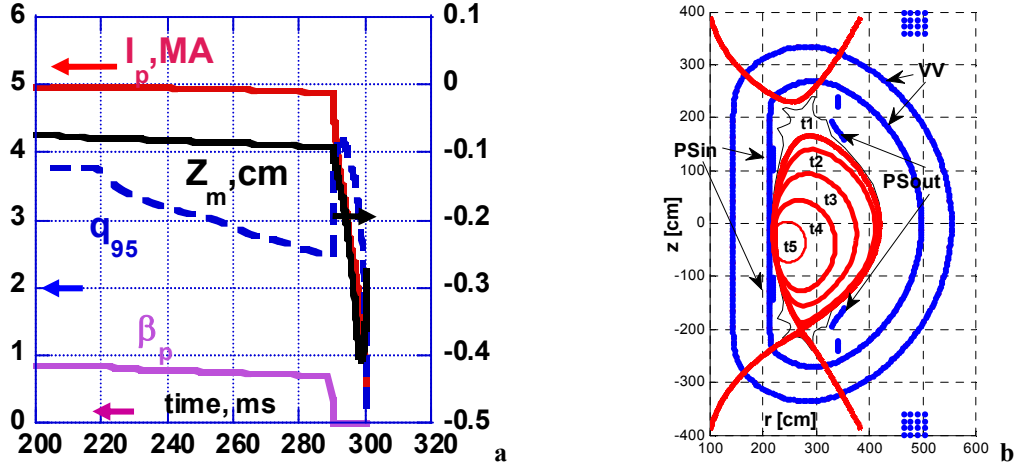


FIG. 3. Time traces of FNS plasma current, vertical coordinate of magnetic axis,  $q_{95}$  and  $\beta_p$  during hot VDE and major disruption (a); evolution of FNS plasma boundary evolution ( $t_1=200$  ms,  $t_2=250$  ms,  $t_3=280$  ms,  $t_4=295$  ms,  $t_5=300$  ms).  $PS_{out}$ ,  $PS_{in}$  are respectively outer and inner passive structures (b)

## 2.1. Sideways forces on the wall during the initial stage of disruption in DEMO-FNS

External kink mode destabilization of the DEMO-FNS tokamak plasma in the process of disruption and the sideways forces acting on the conducting wall due to corresponding eddy currents were investigated. The equilibrium configurations from the DINA simulations of the disruption in DEMO-FNS were considered, in particular the plasma after the thermal quench reduced in size and displaced inside/downward with minor radius about 0.6 m and moderate elongation  $\kappa=1.4$  but with a large total current ( $> 2$  MA) and the safety factor of  $q < 2$  (Fig. 4a). The plasma close enough to the inner side of the vacuum vessel can be stable assuming ideal wall conductivity giving rise to resistive wall mode (RWM) with toroidal wave number  $n = 1$  developing on the resistive wall timescale characteristic to the tokamak disruptions. Using the stability code KINX [4] the conditions for such a one-sided wall stabilization against the ideal kink mode  $n = 1$  (stability gaps) were determined varying the safety factor  $q$  value at the plasma edge (Fig. 4b). The RWM growth rates  $\gamma_{RWM}$  and the eddy currents were calculated in the thin wall approximation. The sideways force acting on the wall was determined as the Lorentz force from the perturbed surface current in the wall and the equilibrium field [5]. The sideways force monotonically increases with the  $\gamma_{RWM}$  and saturates when approaching the ideal wall limit  $\gamma_{RWM} \rightarrow \infty$  ( $q_{edge}$  approaching the right side of the gap) (Fig. 4c). The force is maximal in the stability gap  $q_{edge} > 1$  but its value is quite moderate (below 1 MN) which may be attributed to the absence of the halo/Hiro currents in the DINA disruption modeling with plasma separated from the wall by the vacuum gap. Larger sideways forces can be reached at the next stages of disruptions with plasma/wall contact and/or with more realistic 3D electromagnetic models of conducting wall.

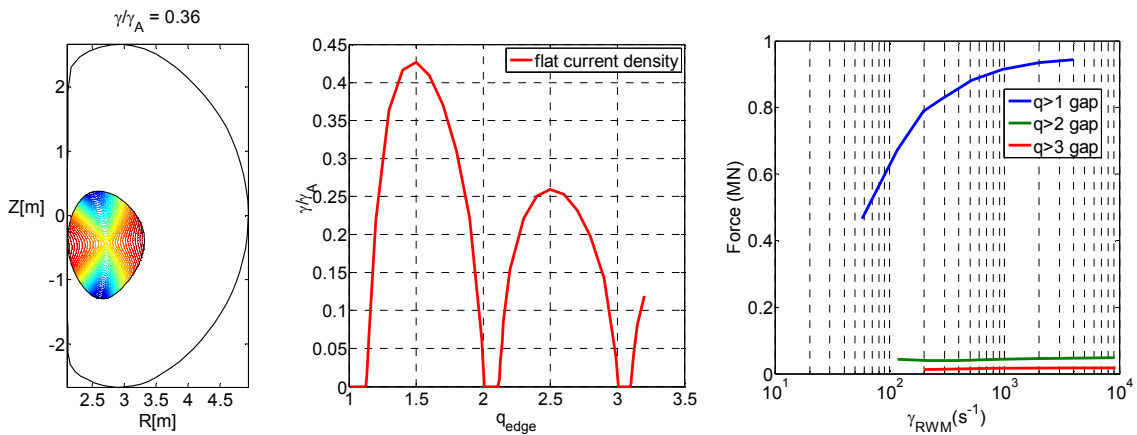


FIG. 4. Plasma position against the TIN vacuum vessel (plasma current  $I_p=2.2$  MA,  $q_{edge}=1.7$ ) and level lines of the plasma displacement normal to magnetic surfaces for unstable  $n = 1$  ideal mode, growth rate  $\gamma / \gamma_A = 0.36$ (a); ideal mode growth rates vs  $q_{edge}$  for flat current density profile(b); values of the sideways force vs  $\gamma_{RWM}$  in three stability gaps assuming normal magnetic field perturbation to be 10% of the equilibrium poloidal field(c).

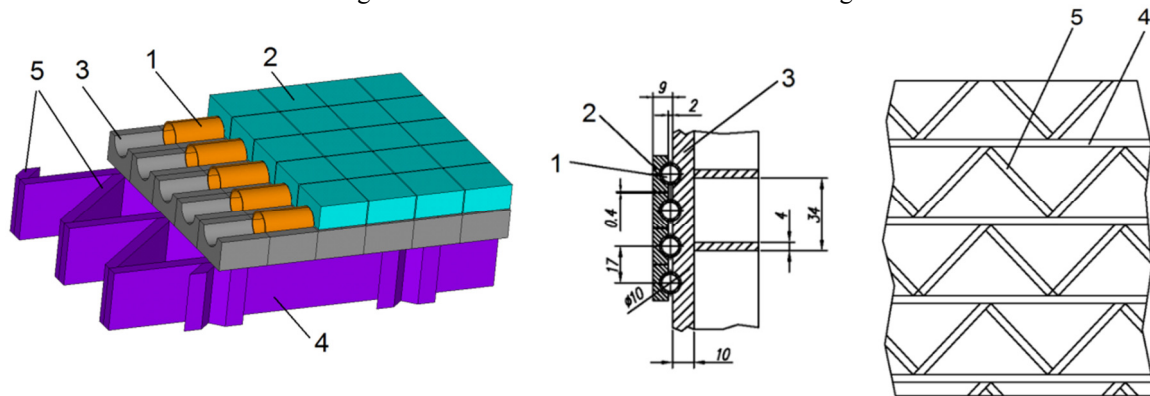
### 3. FIRST WALL AND DIVERTOR DESIGN

#### 3.1. First wall

The FW load-bearing unit was developed capable of withstanding dynamic forces within the range of elastic material behaviour. The design was evaluated taking into account the expected VDE scenario and halo-currents generation during disruption.

Evaluations of neutron damage and He-breeding rate in structural materials were made. For active core with  $k_{\text{eff}} = 0.95$  (hybrid plant case) the neutron damage of FW-materials in dpa is comparable for fusion and fission neutron sources. Meanwhile, the input into the He-breeding rate from fusion neutrons is 4-5 times higher while in spite of the specific heat generation is 8-9 times being lower than that of fission neutrons.

The first wall is divided constructively into 18 autonomous cooling sections (according to the number of toroidal magnetic coils). Each section contains panels of the first wall and two cassettes of the divertor (upper and lower) connected hydraulically together. In addition, the section includes panels of the first wall of the equatorial region of the discharge chamber, which are cooled independently of the cooling of the other panels and divertor cassettes. First wall general view and dimensions are shown in Fig.5.



1 – cooling tube (chrome zirconium bronze), 2 - tile (beryllium), 3 - base (steel 12X18H10T), 4 - stiffener, 5 - crosspieces.

FIG. 5. DEMO-FNS First wall general view and dimensions.

#### 3.2. Concept of lithium vapor box for DEMO-FNS divertor

It has long been recognized that volumetric dissipation of the plasma heat flux within the tokamak SOL is preferable to its localized contact with the divertor target. Volumetric dissipation mitigates both the anticipated very high heat flux and intense particle-induced damage due to sputtering [6]. Tungsten and beryllium as the plasma facing materials of ITER have problems even during steady state plasma operation. Nowadays, a lithium vapour box [7] is being considered as an alternative divertor concept, which can reduce the parallel heat fluxes by 4 orders of magnitude for the DEMO conditions, namely from 20 GW/m<sup>2</sup> down to about 2 MW/m<sup>2</sup> [8], with moderate lithium efflux from the box to the plasma core.

The design of lithium vapour boxes compatible with continuous liquid lithium flow has been developed for DEMO-FNS. The 0D model [8] was improved by taking into account the SOL plasma losses due to the lithium radiation and applied for evaluation of the parameters of the DEMO-FNS lithium vapour box.

The number and dimensions of the boxes, as well as their wall temperatures, were varied to optimize the SOL plasma losses and lithium efflux from the box. The simulations demonstrate that 3-chambered evaporator design is the most optimal since it provides relatively small amount of heat flux onto walls – 1.6 MW/m<sup>2</sup> – within a 30 cm restricted divertor area. However, the lithium efflux to the core plasma is about 3 mg/s, which exceeds required 1 mg/s. Therefore there is a lack of space for both the outer and inner divertor legs in the current DEMO-FNS design.

### 4. MATERIALS STUDIES

The efficiency of the development of structural materials (SM) depends on the level of the available materials science knowledge of the laws and mechanisms for the formation of radiation microstructures, defects and properties of SM. High-dose reactor tests of SM for determination of the degree of the radiation change

(degradation) of their structure and properties are very expensive and time-consuming. Besides, it is difficult to obtain a neutron spectrum in a fission reactor relevant to a fusion reactor environment. To accelerate the development of advanced SM for nuclear fusion technology, theoretical, modeling and simulation researches are necessary both to define parameters of materials and to build physically based models of material properties changes under irradiation in conditions specific for fusion reactors. To this end, the molecular dynamic studies of primary damage for various damage energies  $E^d$  (1 – 50 keV) and material temperatures  $T$  (300 – 900 K) have been performed for bcc metals Fe and V (interatomic interaction potentials [9]), which are the basis of advanced low activation SM for nuclear fusion and fission reactors. The dependences of the number of survived Frenkel pairs after the passage of atomic collision cascades on temperature and damaging energy have been calculated and an analytic expression has been chosen that accurately describes the calculated data:

$$\eta(E^d, T) = B(T) + A \exp\left(-2^{T/T^*} E^d/E^*\right), \quad (1)$$

where  $\eta$  is the number of survived Frenkel pairs normalized to the value given by the NRT equation [10],  $A$ ,  $B$ ,  $T^*$ ,  $E^*$  are fitting parameters. Parameters  $T^*$  and  $E^*$  are the same for Fe and V:  $T^* = 300$  K,  $E^* = 7.2$  keV. Parameter  $A$  only depends on material and equals 0.39 and 0.265 for Fe and V, respectively. Parameter  $B$  for Fe equals 0.25 at all the considered temperatures. For V, it equals 0.26 at 300 K and 0.23 at  $T \geq 600$  K.

The cluster size distributions of the fraction of survived self-interstitial atoms (SIA) and vacancies  $\chi$  are weakly temperature dependent and well described by

$$\chi(n) = \left( n e^{qn} \ln \left[ e^q / (e^q - 1) \right] \right)^{-1}, \quad (2)$$

where  $n$  is the cluster size,  $q$  equals 0.317 and 0.575 for vacancy and SIA clusters in V, respectively, and 0.810 for vacancy clusters in Fe. For SIA clusters in Fe, there is a distinct dependence of  $q$  on  $E^d$ :

$$q(E^d) = 0.385 \ln^{-1} \left( 0.9 + E^d/E_1 \right), \quad (3)$$

where  $E_1 = 1$  keV.

## 5. ELECTROMAGNETIC SYSTEM AND VACUUM VESSEL

Design of electromagnetic system and vacuum vessel was upgraded to provide the integration of new components in the facility. The superconducting magnetic system (SMS) of the DEMO-FNS tokamak includes:

- winding of the toroidal field (TFC), consisting of 18 coils with feeders and supports;
- a partitioned central solenoid (CS), divided by current into five independent modules;
- four pairs of poloidal field coils (PFC) with feeders and power structures;
- three groups of correction coils (CC) (total 18 coils);
- internal and external heat shield;
- interblock unifying structure and supporting components;
- horizontal control field coils (HCFC), providing vertical stability of the plasma, located inside the VV;
- cryostat, containing the entire electromagnetic system.

The design of the DEMO-FNS electromagnetic system is based on the use of conductors such as Cable-in-Conduit Conductors (CICC) made of low-temperature superconductors (LTS), such as Nb<sub>3</sub>Sn, NbTi, and copper and non-magnetic stainless steel. Analysis of the stressed-deformed state of TFC coils has shown that the technically realizable coil design requires placing the winding wire in massive radial plates forming two-layered sections containing the necessary amount of structural material to withstand the mechanical stresses arising during operation (Fig.6.).

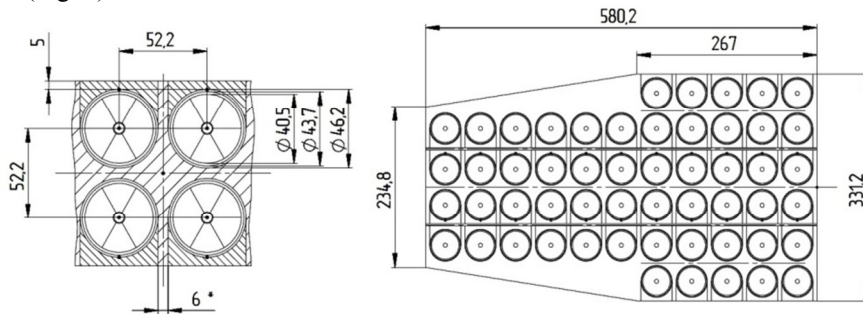


FIG. 6. Cross-section of toroidal field coil inner "leg".

## 6. NBI SYSTEM

Steady-state plasma heating and current drive is provided the NBI system (Fig. 7). Six neutral beam injectors will provide DEMO-FNS machine with additional heating power 30 MW carried by deuterium beams at 500 keV energy. Continuous injection is achieved by a simultaneous operation of 4 injectors (7.5 MW each), while the 5th is stopped for cryopumps regeneration, and the 6th one is envisaged for operational reserve, maintenance or repair. Therefore, with a 30 min stop on regeneration, each injector has 2 hours cycle of operation. The choice of 500keV deuterium beam is proved by beam-plasma calculations [11], as the optimum energy for the beam penetration and plasma heating & current drive - for tangential injection. The designed injectors' layout around the machine is shown in Fig.6. The NB axis is aimed horizontally (with no vertical inclination) at the injection (or 'impact') point which is located at  $R= 3.2/3.4\text{m}$ ,  $Z= -0.5/0.6\text{m}$  (below the tokamak mid-plane). All the 6 injectors are uniformly located around the vacuum vessel with 600 pitch, the injector axis horizontal slope over the vacuum vessel periphery is set to  $\sim 570$  to hit the impact point.

The NB injector geometry for DEMO-FNS is chosen and optimized for the reduced dimensions of injector window to  $0.4 \times 0.8 \text{ m}^2$ , with account of simulations results obtained by BTR4 code [12]. The NBI scheme and general approach are similar to those of ITER H&CD systems, both are based on negative ions ( $\text{D}^-$ ) acceleration and further neutralization on  $\text{D}_2$  gas (with expected neutral yield  $\sim 57\%$ ), yet the change of major parameters (e.g. beam energy and power halving) requires massive and detailed computer simulations. The results currently available also include the beam total losses and thermal loads in various possible operation scenarios, the operational restrictions on the source beam optics and steering, the requirements imposed on the background magnetic field shielding. These results are proposed for engineering design of NBI.

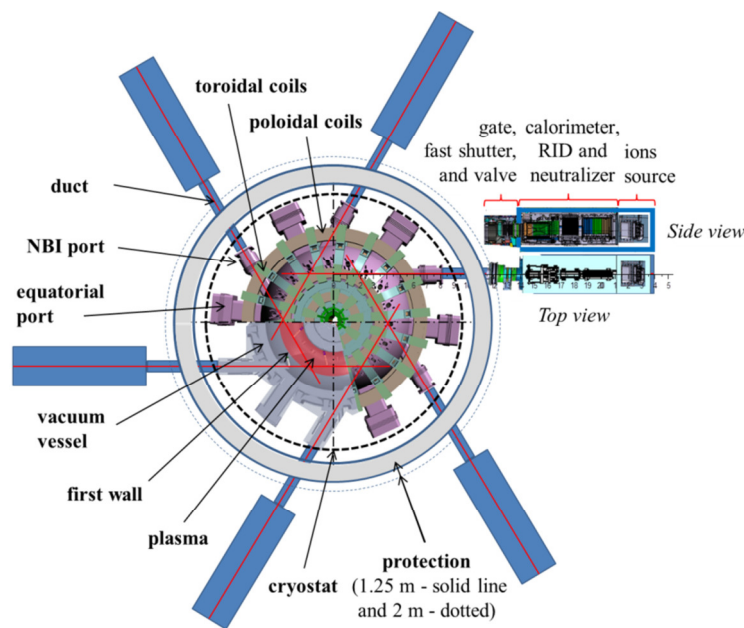


FIG. 7. NBI injectors location relative to DEMO-FNS tokamak.

## 7. USING SUPERCRITICAL $\text{CO}_2$ AS A COOLANT

Advantages of supercritical  $\text{CO}_2$  as a coolant for active cores, TBB, FW and divertor were evaluated. This coolant is attractive due to acceptable pressure ( $\sim 75$  bars) and temperature (up to  $\sim 500^\circ\text{C}$ ) ranges, low activation level in neutron environment, preservation of the hard neutron spectra, and a better compatibility with lithium technologies than that of water coolant. The advantage of supercritical coolants in comparison with liquid coolants is the absence of a heat transfer crisis during boiling. However, in order to remove the heat flux of  $\sim 5 \text{ MW/m}^2$  to achieve acceptable heat transfer coefficients, it is necessary to pump the S- $\text{CO}_2$  coolant with velocity of up to 100 m/s. At such velocities, the regimes with reduced heat transfer will not occur as was observed in [13]. In any case, additional computational and experimental R&D is required.

Activation characteristics evaluation of candidate coolants (Fig.8) showed that that supercritical CO<sub>2</sub> have advantages from point of view of activation and decay heat output and it is possible to organize single-loop cooling system for energy conversion. The fast neutron fluence was assumed to be  $\sim 4.4 \times 10^{21} \text{ cm}^{-2}$  and the total neutron fluence  $\sim 1.3 \times 10^{22} \text{ cm}^{-2}$  due to one year irradiation. The dominant isotopes responsible for the activity of candidate coolants in different cooling periods are indicated nearby the decay curves. Normal water, heavy water and S-CO<sub>2</sub> coolants are characterized by the lowest activation and the fast activity decay. The Sodium (Na) activation via <sup>24</sup>Na and <sup>22</sup>Na prolongs by substantial tritium activity and finally by the <sup>36</sup>Cl-decay. The Molten salts (MS) after irradiation have the highest tritium activity, however this property is positive for tritium breeding. The long-term radionuclides generated from impurities become dominant after hundred years cooling. A characteristic time for <sup>6</sup>Li burning is close to  $\sim 100$  days, so blanket feeding by this isotope should be provided for T-breeding during prolong irradiation campaigns.

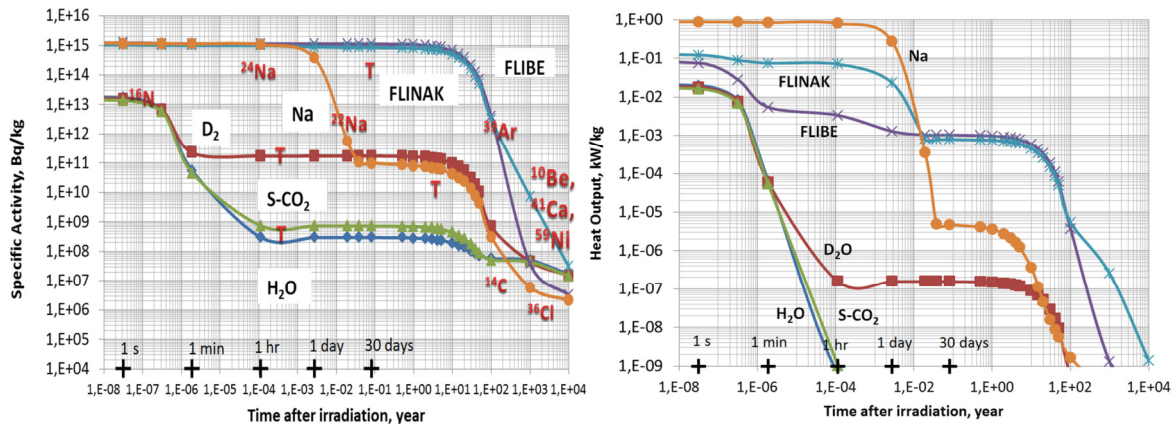


Fig. 8. Specific coolant activity after irradiation during 1 FPY in the CHPP spectra (a); Specific afterheat in coolants after irradiation during 1 FPY in CHPP spectra (b).

Decay curves presented in Fig. 6 show the lowest and comparable levels of specific afterheat for water and CO<sub>2</sub> as well as the highest levels for Na and MS. The short-term afterheat of oxygen containing coolants is provided by <sup>16</sup>N produced through <sup>16</sup>O(n,p)<sup>16</sup>N reaction. <sup>16</sup>N-nucleus decays back to <sup>16</sup>O with T<sub>1/2</sub>=7.12 s emitting β-particle with 2.7 MeV energy and high energy (4.6 MeV) gamma.

## 8. INTERACTION WITH THE NUCLEAR FUEL CYCLE OF RUSSIA'S NUCLEAR POWER INDUSTRY

Analyses of the interaction of DEMO-FNS facility with the nuclear fuel cycle of Russia's nuclear power industry was performed. Two options of implementation of DEMO-FNS technologies dealing with minor actinides burning and enrichment of spent nuclear fuel from RBMK boiling water reactors in GW-scale hybrid power plant operating within Russian atomic energy system were considered. Such a plant could provide fission of MA produced by Russian nuclear power industry so far and in the future. The return of the spent fuel in the closed fuel cycle after enrichment in HPP will reduce the NF-storage and radiotoxicity generated. Closure of the fuel cycle in a two-component system of modern thermal and fast reactors faces the problem of neutron deficit required for the reproduction of fuel nuclides from the raw isotopes U-238 and Th-232.

Potentially capable of reproduction and production of fuel nuclides in the Th-U fuel cycle, thermal reactors have breeding characteristics that are close to reproduction. Fast reactors with U-Pu fuel cycle tend to reduce the reactivity reserve, which practically excludes their support of thermal reactors fuel cycle, as well as reduces the level of production of the FR + TR power system as a whole and decelerate its development. The involvement in the energy system of a system of thermonuclear and hybrid systems with a capacity of about 10% of the total can significantly change the characteristics of the sustainable development of two-component nuclear power.

## 9. CONCLUSIONS

- Fusion power produced by both plasma- and beam-plasma interactions in dependence of the tritium fraction in plasma was calculated. Maximum total fusion power is achieved when tritium fraction is equal to 0.7.
- Electromagnetic loads in the conductive filaments of the VV and the passive structure during major disruption were calculated. With a decrease in q<sub>95</sub> to a critical value q\* = 2.5, a major disruption occurs.

- The FW load-bearing unit was developed capable of withstanding dynamic forces within the range of elastic material behaviour.
- The design of lithium vapour boxes compatible with continuous liquid lithium flow has been developed for DEMO-FNS. The simulations demonstrate that 3-chambered evaporator design is the most optimal since it provides relatively small amount of heat flux onto walls – 1.6 MW/m<sup>2</sup>.
- Molecular dynamic studies of primary damage for various damage energies  $E^d$  (1 – 50 keV) and material temperatures  $T$  (300 – 900 K) have been performed for bcc metals Fe and V.
- The superconducting magnetic system (SMS) of the DEMO-FNS tokamak was upgraded.
- The NB injector geometry for DEMO-FNS is chosen and optimized for the reduced dimensions of injector window to 0.4×0.8 m<sup>2</sup>.
- Thermophysical and activation characteristics of supercritical CO<sub>2</sub> as a coolant were analysed.
- Analyses of the interaction of DEMO-FNS facility with the nuclear fuel cycle of Russia's nuclear power industry was performed.

Further research tasks are the following:

- improvement of simulation models and codes for evaluation of plasma-physical parameters and scenario of the DEMO-FNS tokamak;
- development of models to assess modification of structural and functional materials properties in fusion-fission neutron environment, support of the materials choice;.
- development of neutron-physical model of a hybrid blanket including active core with MA and tritium and fuel nuclides breeding zone;
- re-design and integration of tokamak enabling systems;
- selection of prospective concepts for hybrid fuel cycle and blankets capable of supporting the development of nuclear power industry in Russia using thermal and fast nuclear reactors.

## ACKNOWLEDGEMENTS

The work was partially supported by the State Atomic Energy Corporation ROSATOM.

## REFERENCES

- [1] B.V. Kuteev et al., 2015 Nucl. Fusion **55** 073035 <https://doi.org/10.1088/0029-5515/55/7/073035>.
- [2] B.V. Kuteev, Yu.S. Shpanskiy and DEMO-FNS Team, 2017 Nucl. Fusion **57** 076039 <https://doi.org/10.1088/1741-4326/aa6dcb>
- [3] V.E. Lukash., V.N. Dokuka., R.R. Khayrutdinov Computer program complex “DINA” in Matlab system for solving problems of tokamak plasma control // PNST ser. “Nuclear Fusion”. 2004. No 1 pp. 3-10.
- [4] L. Degtyarev et al. The KINX ideal MHD stability code for axisymmetric plasmas with separatrix. Computer Physics Communications. Volume 103, Issue 1, June 1997, Pages 10-27
- [5] D.V. Mironov, V.D. Pustovitov, Phys. Plasmas 24 (2017) 092508.
- [6] J. Wesson et al., Clarendon Press Oxford, “Tokamaks”, 2004
- [7] Y. Nagayama, J. Fusion Engineering and Design 84 (2009) 1380-1383
- [8] R.J. Goldston, R. Myers and J. Schwartz, J. Phys. Scr. T167 (2016) 014017
- [9] A.B. Sivak, V.A. Romanov, V.M. Chernov, Influence of stress fields of dislocations on formation and spatial stability of point defects (elastic dipoles) in V and Fe crystals, J. Nucl. Mater. 323 (2003) 380-387.
- [10] M.J. Norgett, M.T. Robinson, I.M. Torrens, A proposed method of calculating displacement dose rates. Nucl. Eng. Des. 33 (1975) 50–54.
- [11] A.Yu. Dnestrovskij et al. Integrated modelling of DEMO-FNS current ramp up scenario and steady state regime. — Nucl. Fusion, 2015, vol. 55, p. 063007; doi 10.1088/0029- 5515/55/6/063007.
- [12] S.S. Ananyev, E.D. Dlougach, B.V. Kuteev, A.A. Panasenkov, Modeling and optimization of neutral beam injectors for fusion neutron source DEMO-FNS – VANT/ Nuclear fusion serie, 2018, Vol. 41, issue 3, p.57-79
- [13] V.A. Kurganov, Heat Exchange in Pipes at Coolant’s Supercritical Pressures. Some Results of Scientific Research (in Russian). Proceedings of the 4th RNHTC (2006). Volume 1. Plenary and general reports. Presentations at round table. Pages 74-83.